FATIGUE CRACK PROPAGATION BEHAVIOR OF 2091 T8 AND 2024 T3 UNDER CONSTANT AND VARIABLE AMPLITUDE LOADING

N. OHRLOFF, A. GYSLER[*] and G. LÜTJERING[*]

*Messerschmitt-Bölkow-Blohm GmbH, Kreetslag 10,
D-2103 Hamburg 95, F.R.G.*
[*]*Metallkunde und Werkstofftechnik, Technishe Universität
Hamburg-Harburg, Harburger Schlosstrasse 20, Postfach 901403,
D-2100 Hamburg 90, F.R.G*

ABSTRACT

The fatigue crack propagation behavior of the damage tolerant 2091 T8 was compared with that of 2024 T3. Constant amplitude tests were performed in vacuum, air, and NaCl solution at R = 0.175 and in air at R = 0.7. The variable amplitude tests included periodic underloads superimposed on constant amplitude tests at R = 0.7, and periodic overloads in combination with low R-ratio tests. In general it was found that the crack propagation resistance of 2091 was slightly inferior in the lower ΔK-region as compared to 2024, but somewhat better at higher ΔK-values. For both alloys predicted propagation rates based on constant amplitude tests were lower than the experimentally measured values with periodic underloads. Periodic overloads resulted in crack growth retardation.

INTRODUCTION

The new low density, high stiffness Li-containing Al-alloys are considered as attractive materials to replace some of the conventional Al-alloys in future aircraft generations. In comparison to the competing advanced composite materials the Al-Li base alloys offer advantages for the aircraft industry and the airline companies, for example similar manufacturing methods as for conventional Al-alloys and only minor adjustments for both inspection and repair procedures. Besides the still not completely solved problems of lower ductility and fracture toughness values of Li-containing alloys in comparison to conventional Al-alloys, more experimental results seem to be necessary with regard to the resistance against fatigue crack propagation, especially under variable amplitude loading conditions.

The objective of the present work was to compare the fatigue crack propagation behavior of one of the new damage tolerant Li-containing Al-alloys 2091 T8 with that of the conventional 2024 T3 alloy under constant and variable amplitude loading.

EXPERIMENTAL PROCEDURE

The alloy 2091 was supplied by Pechiney in the form of 1.6 mm thick sheet material (unclad) in the T8 condition (15 min 530°C/WQ, 1-3% stretching, 12h 135°C). The 2024 T3 alloy was tested as 2 mm alclad sheet material for comparison. The composition of 2091 and typical values for 2024 are shown in Table 1.

All mechanical tests reported here were performed with the loading axis parallel to the rolling direction of the sheet material. Tensile tests were done on flat specimens with gage dimensions of 12.5 mm width and 52 mm length (ASTM E 8-83). Crack propagation tests were conducted on CCT-specimens with dimension of 30 mm x 90 mm or 160 mm x 400 mm using load-controlled servo-hydraulic testing machines at a frequency of 30 Hz. Crack propagation rates, starting from notches prepared by spark erosion cutting, were monitored with a travelling microscope.

Table 1: Chemical compositions of 2091 and 2024 (wt.%)

	Cu	Li	Mg	Zr	Mn	Fe	Si	Ti	Na
2091	2.0	1.9	1.6	0.08	–	0.03	0.02	0.02	0.0002
2024	4.4	–	1.5	<0.25	0.6	≤0.5	≤0.5	–	–

Constant amplitude tests were performed on both alloys at R = 0.175 in vacuum, laboratory air, and 3.5 % NaCl solution to study the effect of environment, and in addition at R = 0.7 in air. Three types of variable amplitude tests were carried out on both alloys: Type B, a periodic sequence consisting of 10 cycles with R = 0.7 followed by 1 "underload" cycle with R = 0.175 (keeping K_{max} constant), Type C, composed of a periodic sequence of 1 cycle with R = 0.175 followed by 1 cycle with R = 0.366 (keeping K_{min} constant), and Type D, a periodic sequence having 999 blocks of Type C and 1 overload block of Type C but with a 20 % higher K_{max} value.

All da/dN-ΔK curves presented in this paper were obtained by fitting the experimentally determined data points using the incremental poly-nomial method (ASTM E 647-83).

EXPERIMENTAL RESULTS

The tensile properties ($\sigma_{0.2}$, UTS, ε_F) of 2091 T8 are listed in Table 2 including with results of 2024 T3 for comparison. All three values were lower for 2091 as compared to 2024, for example $\sigma_{0.2}$ was 330 MPa for 2091 and 380 MPa for 2024.

Table 2: Tensile properties of 2091 T8 and 2024 T3

	$\sigma_{0.2}$ (MPa)	UTS (MPa)	$\varepsilon_F = \ln A_O/A_F$
2091 T8	330	442	0.22
2024 T3	380	480	0.29

The fatigue crack propagation results (da/dN vs. ΔK) of 2091 T8 and 2024 T3 under constant amplitude loading at R = 0.175 are shown in Figure 1 for three different environmental conditions (vacuum, air, NaCl solution). These curves show the well known effect of a decreasing crack propagation resistance with increasing environmental aggres-siveness. For 2024 all three curves are fairly straight and also for 2091 in vacuum and NaCl solution. However for 2091 tested in air a pronounced change in the shape of the da/dN-ΔK curve was observed (Figure 1) approaching in the lower ΔK-regime the curve obtained in NaCl and converging in the high ΔK-region with the vacuum curve. It should be mentioned that for 2091 tested in air an unusual amount of scatter in da/dN was observed in the intermediate ΔK-regime (around 9 MPa$\sqrt{m}$).
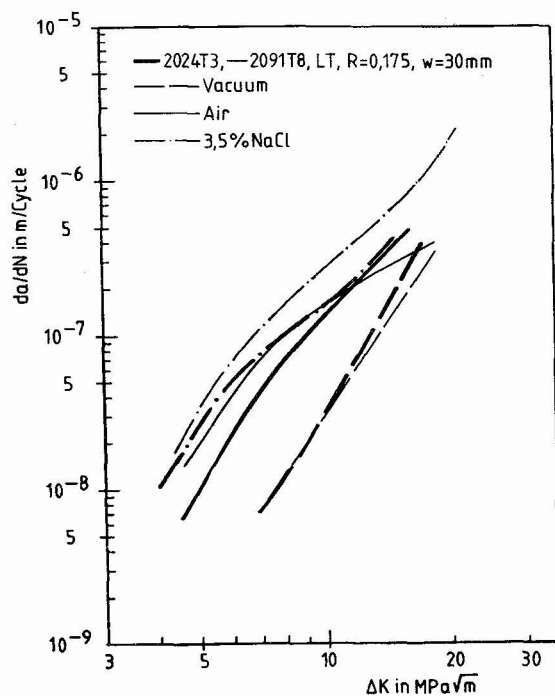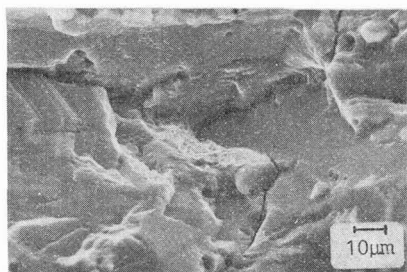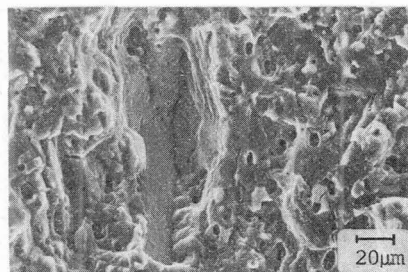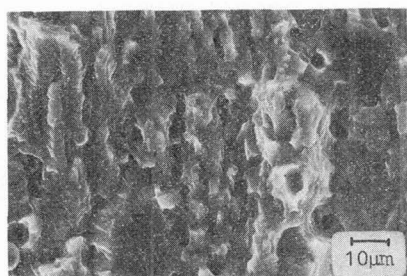
Figure 1:
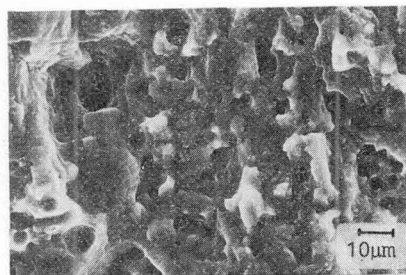Influence of environment
on fatigue growth rates of
2024 T3 and 2091 T8

a) Vacuum, $\Delta K = 7$ MPa$\cdot$m$^{1/2}$

b) Air, $\Delta K = 14$ MPa$\cdot$m$^{1/2}$

c) Air, $\Delta K = 9$ MPa$\cdot$m$^{1/2}$

d) NaCl, $\Delta K = 14$ MPa$\cdot$m$^{1/2}$

Figure 2: Fractographs of 2091 T8, R = 0.175

The results of fracture surface studies are summarized in Figure 2 for
2091. In vacuum fatigue crack propagation occurred within the whole
ΔK-region in a highly crystallographic manner mostly along single slip
planes within one grain at low ΔK (Fig. 2a) and to a lesser extent
along grain boundaries. In NaCl solution cracks also propagated mostly
in a transgranular mode but the propagation direction changed fre-
quently from one plane to the other within one grain (Fig. 2d). In air
the crack propagation mechanism in the low ΔK-regime was similar (Fig.
2c) as observed in NaCl solution (compare Fig. 2d), while in the
higher ΔK-region (above about 9 MPa √m) a transition was observed
exhibiting portions of trans- or intergranular fracture modes (Fig.
2b) similar as described for the vacuum tests.

For 2024 the fracture surface appearance in vacuum also exhibited slip
band fracture, however along several slip systems per grain already in
the lower ΔK-regime, and in contrast to 2091 showed increasing por-
tions of dimple rupture with increasing ΔK. In NaCl solution and in
air 2024 exhibited a transgranular fracture mode similar as observed
for 2091 in NaCl solution (compare Figure 2d).

The influence of mean stress on da/dN-ΔK for 2091 and 2024 in air is
shown in Figure 3 by comparing curves obtained for R = 0.175 and
R = 0.7. Increasing the mean stress resulted in a nearly parallel
shift of the curves to higher propagation rates (about a factor of 2)
for both alloys without changing the shape of the curves. While the
alloy 2091 exhibited for both R-ratios the already described pro-
nounced sigmoidal shape, the curves for 2024 were fairly smooth within
the measured ΔK-regime (Fig. 3). The crack propagation resistance of
2091 in comparison to 2024 is lower in the ΔK-regime below about 10
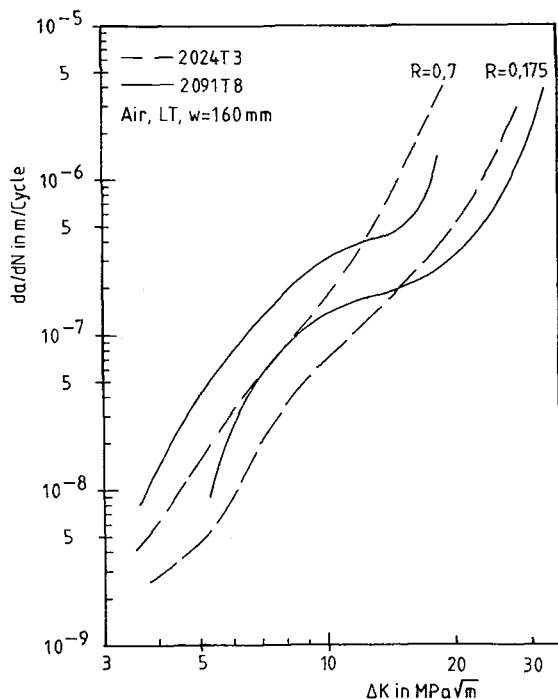MPa √m and higher in the upper ΔK-region (Fig. 3).

Figure 3:
Influence of mean stress on
fatigue crack growth rates
of 2024 T3 and 2091 T8

The effect of variable amplitude loading according to Type B (10 cycles with R = 0.7, 1 cycle with R = 0.175) on da/dN-ΔK (ΔK calculated for R = 0.7) is shown in Figure 4 for 2091 and 2024. It can be seen that in the ΔK-regime below about 4 MPa $\sqrt{m}$ the resistance against crack propagation was lower for 2091 as compared to 2024, while this ranking was reversed at higher ΔK-values. It should be noted that the fatigue crack propagation curve of alloy 2091 for this type of variable amplitude loading did not show the same pronounced sigmoidal shape as observed for constant amplitude loading (compare Figures 4 and 3). Also shown in Figure 4 are predicted da/dN-ΔK curves calculated on a linear basis from the results of constant amplitude tests in Figure 3. For both alloys the predicted da/dN values are always lower than the experimentally measured propagation rates (Fig. 4).

The results of variable amplitude loading conditions according to Type C are shown in Figure 5 for 2091 and 2024, together with curves obtained for the same loading history but with periodic overloads (Type D: 999 blocks Type C + 1 block with 20% overload of Type C). It can be seen that the addition of one 20% higher overload block per 1000 blocks resulted for both alloys in a considerable amount of crack propagation retardation. This effect was more pronounced in the higher ΔK_{max}-regime. It also should be mentioned that this type of variable amplitude loading again resulted in pronounced sigmoidal shapes of the da/dN-ΔK_{max} curves for the alloy 2091 (Fig. 5).

DISCUSSION

It is well known that Li-containing Al-alloys in underaged conditions (such as 2091 T8) exhibit pronounced slip band formation during plastic deformation [1]. The lower ductility of 2091 even at a lower yield stress in comparison to 2024 (Table 2) is a result of such planar slip behavior.

A further consequence of the severe slip band formation in 2091 was the observation that fatigue crack propagation in vacuum occurred mainly along these slip bands (Figure 2a) even at high ΔK-values, while for 2024 increasing dimple portions were observed with increasing ΔK due to the more homogeneous deformation mode. In the aggressive NaCl solution the resistance against fatigue crack propagation of both alloys dropped significantly (Fig. 1). Crack propagation occurred in the whole ΔK-regime along several slip systems within one grain in both alloys (Fig. 2d). It is thought that hydrogen atoms, swept into the slip bands by moving dislocations, are responsible for this transgranular fracture mode and the low crack propagation resistance.

In air the fracture mode in the lower ΔK-regime of 2091 and 2024 was similar to that observed in NaCl solution (compare Figures 2c and 2d), resulting again in relatively low crack propagation resistance values (Figure 1). While this environmentally induced propagation mode (water vapor) persisted in the whole ΔK-regime for 2024, a gradual transition in fracture mode was observed for 2091 with increasing ΔK towards that one observed for tests in vacuum (compare Figures 2b and 2a). One of the reasons responsible for this change in fracture mode might be due to the longer slip distances in 2091 causing microcrack nucleation within slip bands or at grain boundaries ahead of the crack tip. The pronounced sigmoidal shape of the da/dN-ΔK curve of 2091 in air (Figure 1), which seems to be characteristic for Li-containing Al-alloys [2-5], obviously results from the observed change in fracture mode with increasing ΔK. This difference in the shape of the da/dN-ΔK curves between 2091 and 2024 was not only observed at
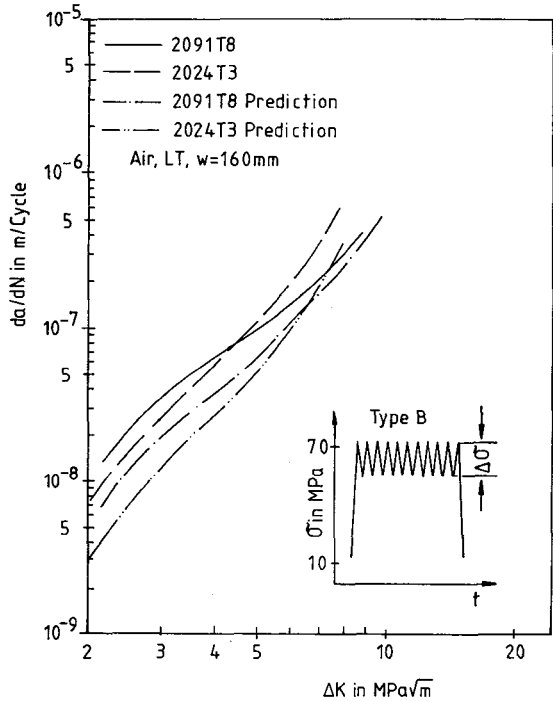
Figure 4:
Influence of periodic
underloads on fatigue
crack growth rates of
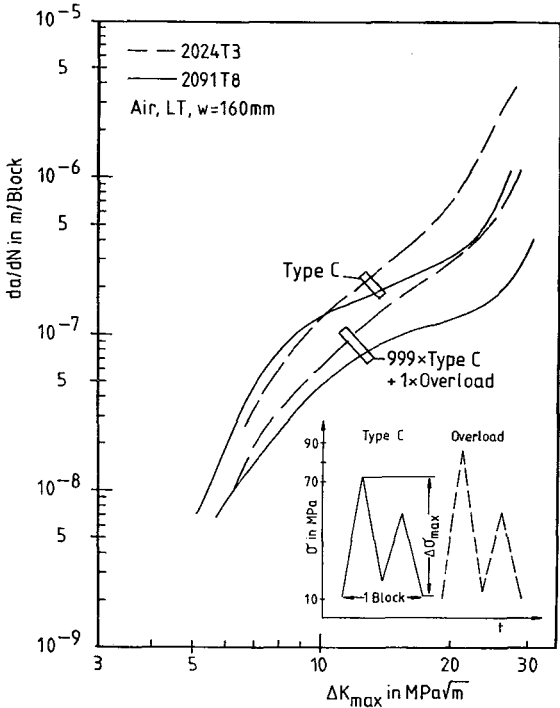2024 T3 and 2091 T8

Figure 5:
Variable amplitude fatigue
crack growth rates without
and with periodic over-
loads

R = 0.175 but also at R = 0.7 (Figure 3), resulting in a somewhat superior fatigue crack propagation resistance of 2091 at higher ΔK-values in comparison to 2024.

Variable amplitude loading conditions of type B (10 cycles with R = 0.7 followed by 1 cycle with R = 0.175) resulted in considerable crack propagation acceleration for both alloys (compare Figure 4 with Figure 3 at R = 0.7) [6]. It is thought that in addition to crack closure effects crack tip sharpening during each cycle with the low K_{min}-value contributes to the observed acceleration. Predicted growth rates on the basis of constant amplitude tests (Figure 3) resulted in lower da/dN-values for both alloys (Figure 4), because this calculation cannot account for any sequential effects. It should be mentioned that for this type of loading no change in fracture mode was observed for 2091, because the ΔK-values were not high enough (compare Figures 4 and 3).

Periodic overloads (999 blocks of type C followed by 1 overload block) caused crack growth retardation for both alloys (Figure 5) [5]. Since for 2091 again pronounced sigmoidal shapes of the da/dN-ΔK curves were observed, the resistance against crack growth of the Li-containing Al-alloy under both of these types of variable amplitude loading conditions was superior in the higher ΔK-regime as compared to 2024. The observed change in fracture mode for 2091, which is responsible for the sigmoidal shape of the da/dN-ΔK curves, is in agreement with the higher ΔK-values (Figure 5), necessary for the transition from the environmental induced to the vacuum fracture mode.

Finally it should be emphasized that for prediction of crack growth under variable amplitude loading conditions the crack growth accelerating effects of underloads as well as the crack growth retardation effects of overloads have to be taken into consideration.

ACKNOWLEDGEMENT

REFERENCES

[1] K.V. Jata and E.A. Starke, Jr., Metallurgical Transaction 17A (1986) 1011.

[2] J. Petit, S. Suresh, A.K. Vasudevan and R.C. Malcom, in "Aluminum-Lithium Alloys III", pp. 257, The Institute of Metals, London, 1986.

[3] M. Peters, V. Bachmann and K. Welpmann, 4th International Al-Li Conference, Paris, 1987.

[4] K. Welpmann, H. Buhl, R. Braun and M. Peters, 4th International Al-Li Conference, Paris, 1987.

[5] R.J.H. Wanhill, W.G.J. 't Hart, L. Schra and H.J. Kolkman, 4th International Al-Li Conference, Paris, 1987.

[6] R.J.H. Wanhill, Metallurgical Transactions 6A (1975) 1587.